Optimization of Single-Phase Induction Motor for Improved Optimal Control

OTOGWUNG, O.M[1], IDONIBUOYEOBU D.C[2], BRAIDE, S.L[3]
[1, 2, 3] *Department of Electrical Engineering, Rivers State University, Port Harcourt, Nigeria*.

Abstract- ***The single-phase induction motors are mainly applied or used at home to drive mechanical loads. One of the problems of induction motors is the frequency of the supply voltage is affected by the load. This paper focuses on optimization of a single-phase induction motors for improved optimal control using a variable capacitance for a 1hp, 50Hz, 4 pole machine. MATLAB/Simulink framework was structured to characterize the physical representation of the study under investigation using a d-q equivalent circuit reference frame technique for the purpose of modeling simulation. The machine input data was used and translated into machine variable. The technique establishes and characterizes the voltage equation, current equations, and torque equation on the view to identify and improve the performance of the motor during the starting phase of the machine. The simulation results show that higher capacitance of capacitor is required in the auxiliary phase circuit. The machines are loaded gradually to drive at constant and varying conditions, to measure and identify performances. The existing capacity of the capacitor (capacitance) were doubled for purpose of simulations of transient and steady state performance of the single-phase induction motor (SPIM) with the rated capacity of 32µF in order to improve the optimal performance of the machine in terms of speed, time etc. thereby making more productions. The results showed that the switching capacitor of the SPIM uses larger starting capacitor value of 32µF, making the machine to reach steady-state operation, this means that increasing the capacity of the load at varying time with the speed of dual capacitor of SPIM, will significantly improve the production time in order to make more profit and performance. Evidently, the dual capacitor placements produce higher torque both in transient and steady state scenarios, including the efficiency of the dual capacitor motor particularly in the steady state reaching up to about 85% of the speed of the motor. Initially, the supply voltage for stator and rotor operates at 230V, for Stator scenario, when the time is = 0.1 seconds, the motor has no external load, because the voltage reduced to -220V at no-load value. When the time operates at t= 0.02 Second, the supply voltage increases to +220V. Similarly, When the time operates at t= 0.03 Second, the supply voltage decreases to -220V then finally, When the time operates at t= 0.04 Second, the supply voltage increases to +220V. The results show that the supply voltages operate at 230V and vary the load torque to find the maximum torque at this reduced voltage.***

Indexed Terms- ***Voltage equation, Single induction motor, machine variable, Dual capacitor, torque equation.***

I. INTRODUCTION

Induction motors are the most widely used in domestic, commercial and various industrial applications. Particularly, the squirrel cage type is characterized by its simplicity, robustness and low cost, which has always made it very attractive, and it has therefore captured the leading place in industrial sectors. As a result of its extensive use in the industry, induction motors consume a considerable percentage of the overall produced electrical energy [1]. The minimization of electrical energy consumption through a better motor design becomes a major concern. Many practical optimization problems in optimization of the electromagnetic devices have mixed (continuous and discrete) variables and discontinuities in search space [2]. If the standard non-linear programming (NLP) techniques were to be used in such cases, then they would be computationally very expensive and inefficient. Some applications utilizing the standard NLP techniques include the design optimization of induction motor.

Single-phase induction motors (SPIMs) are widely used in many domestic appliances and light-duty industrial applications where single-phase power is not readily available. A SPIM is provided with two stator windings (i.e., main and auxiliary winding) and a squirrel cage rotor. The two windings, which are in space quadrature, usually have different impedances and are fed from a common single-phase source. The most common SPIM types are split-phase, capacitor-start, and capacitor-start-and-run. The split-phase motors have the problem of poor starting torque that is solved by using a capacitor-start in series with the auxiliary winding [3]. The start capacitor may be disconnected after starting by means of a centrifugal switch. In capacitor-start-and-run SPIMs, one more capacitor is permanently connected to the auxiliary winding for improving motor performance. The function of the capacitors is to generate a leading phase current in the auxiliary winding so that the motor can produce a sufficiently high starting torque and operate as a balanced two-phase machine. However, the impedance of the auxiliary winding changes considerably from starting to running mode and also depends on load condition during the period of normal operation. Therefore, symmetrical and balanced operation of an SPIM cannot be ensured by just altering the two fixed value capacitors according to mode operation. Additionally, since hundreds of thousands SPIMs are being used in various applications, the requirements of high efficiency and robust performance are of great importance.

The optimization of the electrical motors with respect to the efficiency improvement based on the evaluation of the mechanical parameters and scaling laws at single-phase induction motors has been analyzed. Optimization of single-phase capacitor motors has been investigated with triac-based voltage controller or in the drive configuration with Hall sensor [4]. Over the years, different optimization algorithms have been employed for the optimization of the single-phase motors such as particle swarm optimization, surrogate fled-circuit model, or genetic algorithms applied in single- or multi-objective optimization models. Hybrid algorithm consisting of the particle swarm optimization and the genetic algorithms was applied in determining the optimal operating point of the two-phase motors regarding the increased efficiency and reduced torque ripple. The last one presents the optimal motor operating point after optimization has been done and efficiency factor has been calculated by FEM (Finite Element Method). Artificial neural network controller has enhanced the efficiency and the dynamic responses of single-phase induction motors particularly when the motors are operated at partial load. Optimization of the induction motors advances further with the usage of fuzzy logic-based controller acting as a supervisor in reducing flux levels during the transients and contributes to the efficiency improving of the dynamic operating modes. Maximization of the efficiency at the induction motors is achieved by introducing mechanical improvement in stator and rotor core, i.e., slits in the middle of the stator and the rotor teeth.

Although advances in technology have enabled the rapid employment of adjustable frequency ac supplies for single-phase ac machines, they have not been widely used in the single-phase counterparts. Inverter-fed SPIMs with continuously variable speed may exhibit improved performance. However, their applications are limited in high demanding systems, due to the complexity and high cost [5]. Additionally, the control in SPIMs does not provide constant torque operation for the entire motor speed range since the maximum available torque rapidly decays below half of the base frequency. Speed adjustment of SPIMs is mainly accomplished by using tapped windings or control of the supplied voltage. Specifically, the rotational speed is adjusted through voltage control, by increasing the slip or by multispeed operation at fixed distinct speed values. From the survey of published literature, it is revealed that there is a need for a simple, reliable, and cost-effective optimal efficiency controlled SPIM drive that can be easily implemented to any retrofit applications.

Worldwide, around 70% of total electricity is consumed by electric motor and nearly 90% of this consumption is done with ac single-phase induction motors in the power range from 0.75 kW to 750 kW [6]. Additionally, the expansion rate of the motor load within the industrial sector is estimated to be 1.5% and for the tertiary sector 2.2%. As per the statistical data available the squirrel cage induction motors up to 52 kW capacities are the major consumers of electricity. Because of high energy consumption and the very large number of installed units, even a small increase

in efficiency improvement can have major impact on the total electrical energy consumptions [7]. In every 1% improvement in motor efficiency might lead to savings of over $1 billion per annum in energy prices, 6-10 million tons (5.4-9.1 million tons) less per annum of combusted coal and close to 15-20million tons (13.6-18.1 million tons) less greenhouse emission into the atmosphere. It is calculated that a full implementation of efficiency improvement choices might scale back worldwide electricity demand up to 7 percent. Motors with low efficiency waste plenty of energy that will increase its operational price. Studies conducted by the Electric Power Research Institute reveal that over 60% of industrial motors are operating below 60% of their rated load capacity [8].

In different word, 40% of commercial motors have endlessly wasting the electrical energy for about 15%. Although, the motors are generally economical, idling, cyclic, gently loaded or outsized motors consume a lot of power than needed even when they are not working. It is estimated that if all countries begin to adopt best Minimum Energy Performance Standards (MEPS) for all motors employed in operation, then by the year 2035 we are able to save up-to 325 terawatt hours of annual electrical energy hence, reduction of CO2 by 206 million tons. Thus, it is of prime importance to focus on efficiency due to economic and environmental reasons.

II. STATEMENT OF THE PROBLEM

Induction motors are workhorse of all industries due to its power quantitative relationship dependability even in low worth and nearly maintenance free operation in its life cycle. However, motors with low efficiency waste a lot of energy that will increase its operational cost. As a result of high energy consumption and the very large number of installed units, even a small increase in efficiency improvement can have major impact on the entire energy consumptions.

The users or operators have to come up with various approaches to improve efficiency and torque of a single-phase induction motor (SPIM) so that less energy will be consumed by the motor, thereby decreasing operational costs.

III. AIM OF THE STUDY

The aim of this work is to analyze the optimization of single-phase induction motors for improved optimal control

The objectives are of this work are outlined as:

i. To develop models for the behaviour of single-phase induction motor.
ii. To develop the equivalent circuit of a single-phase induction motor in d-q axis.
iii. To determine the effect of capacitor variation on the (supply voltage, motor torque, angular speed, stator current and rotor current) of the single-phase motor.
iv. To determine the single-phase capacitor run induction motors of different components.

IV. LITERATURE REVIEW

According to [3] they used an Artificial Neural Network controller in synthesis and training offline to determine the optimal flux level that achieves maximum drive efficiency. Based on the steady state induction motor model, the motor power losses are calculated as a training data. Their proposed neural control model has one input layer, two hidden layer and one output layer. The input layer consists of speed and load torque reference signals.

According to [9] they found out that when the drive system is in a steady-state condition, the efficiency-optimization is enabled and the fuzzy search controller begins to search the optimal flux. When the load torque or the command speed suddenly changes, rated flux operation is established. The low frequency pulsating torque due to decrementation of rotor flux is compensated in a feed-forward manner

According to [10] they proposed the search controller in the scalar control model by adaptively obtaining the stator voltage per hertz ratio use fuzzy logic controller. Input of the fuzzy logic controller is the change of input power and volt per hertz ratio. The output is the new change of volt per hertz ratio. Another authors proposed the search controller in the scalar control model by adaptively reducing the stator voltage reference with the use of a fuzzy logic controller. The torque pulsation problem is overcome with the help of

feed-forward pulsating torque compensation. Input of the fuzzy logic controller is stator voltage and input power and the output is the voltage reference compensator

According to [11] they proposed search based on the "Rosenbrock" method, which determines the flux level that results in the minimum input power. Once this optimal flux level has been found, this information is utilized to update the rule base of a fuzzy controller that plays the role of an implicit mathematical model of the system. Initially, for any load condition, the rule base yields the rated flux value. As the optimum points associated with the usual operating conditions (given by the required speeds and load torques) are identified by the SC, the rule base is progressively updated such that the fuzzy controller learns to model the optimal operating conditions for the entire torque speed plane. As the machine parameters are subject to change during operation, the SC is kept active to track possible minor deviation of the optimum point, thus ensuring true optimal efficiency operation.

According to [12] they conducted a performance analysis of a single-phase induction motor as a result of change in design parameters using analytical approach. Their studies focus on an induction motor without core loss. Their studies revealed that increase in stator resistance can cause the motor to develop more jerks on startup, change the shape of the run up speed and torque.

According to [13] they examined the optimal capacitance selection for a wind driven self-excited reluctance generator under varying wind speed and load conditions. The research presented methodology to determine and select a suitable excitation capacitance value for a wind-drive self-excited reluctance generator (WDSERG) which produces a constant output voltage under changing wind speed and connected load. A steady state mathematical model of the generator was developed from the dynamic model of self-excited reluctance generator (SERG) and phasor diagram. The model developed is used to an algorithm that searches for the optimum excitation capacitance which produces a derived output voltage level for any given wind speed and load within the operating limits of the (WDSERG).

According to [14] he examined a dual stator winding induction machine, the researchers detailed an overview of the topological variations of multi-winding induction machines (IMs) and drives. They restricted their research work to IMs having two distributed windings on the stator and a brushless rotor. The mathematical modeling techniques and control algorithms available in the literature are highlighted. Being magnet-less and brushless the dual stator winding IM is reliable, its maintenance free and economic.

V. MATERIALS AND METHOD

3.1 Materials Used

The materials used in this research are as follows:

i. Matrix laboratory/Simulink Software
ii. 1Hp of single-phase induction motor
iii. 32µF Capacitor
iv. Parameters of the induction motor

3.2 Description of the Method Used

The single-phase induction motor is asymmetrical due to the unequal resistances and inductances of the main and auxiliary windings. To obtain the model equation of the motor with constant parameters (voltage, current, and flux), All the variables are transformed to the stationary reference frame (*d*-*q*) fixed to the stator.

Simulation is conducted using MATLAB/Simulink software for machine study based on the formulate equations. The model equation for the MATLAB program is based on analytical approach and validated using numerical techniques.

The single-phase induction machine (SPIM), without its start-up and running capacitors, is treated as an asymmetric two-phase machine. The auxiliary and main windings are accessible and are in quadrature.

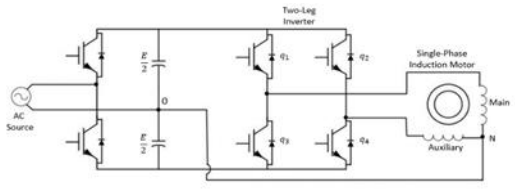

Figure 3.1: The single-phase induction machine (SPIM) of a half-bridge rectifier with a divided DC

bus, two filter capacitors, and a two-leg inverter that supplies the motor windings.

3.3 Machine Model

The circuit diagram shows the machine model.

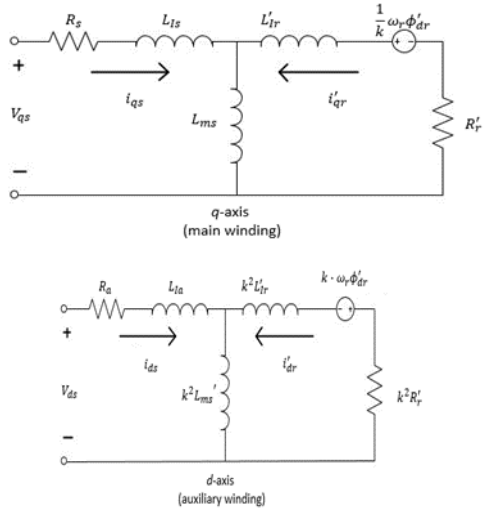

Figure 3.2: Auxiliary and main stator windings

3.3.1 Model of the motor with constant parameters (voltage)

The equations that define the voltage for the model (in the stationary reference frame *d*-*q*) are:

$$V_{qs} = R_s i_{qs} + \frac{d\emptyset_{qs}}{dt} \quad (3.1)$$

$$V_{ds} = R_a i_{ds} + \frac{d\emptyset_{\mathrm{ds}}}{dt} \quad (3.2)$$

$$0 = R^I r i^I_{qr} + \frac{d\emptyset^I{}_{qr}}{dt} - \frac{1}{k}.\omega_r \emptyset^I_{qr} \quad (3.3)$$

$$0 = k^2 R^I r i^I_{dr} + \frac{d\emptyset^I}{dt} - k.\omega_r \emptyset^I_{dr} \quad (3.4)$$

And

$$k = \frac{N_a}{N_m}, \quad (3.5)$$

Where

V_{qs} is the *q*-axis stator voltage in Volts

R_s is the main stator resistance in Ohms

i_{qs} is the *q*-axis stator current in Amps

$\emptyset_{qs}$ is the *q*-axis stator flux linkage in Webbers

V_{ds} is the *d*-axis stator voltage in Metres

R_a is the auxiliary stator resistance in Ohms

i_{ds} is the *d*-axis stator current in Amps

$\emptyset_{\mathrm{ds}}$ is the *d*-axis stator flux linkage in Webbers

$R^I r$ is the rotor winding resistance referred to the main stator winding in Ohms

i^I_{qr} is the *q*-axis rotor current referred to the main stator winding in Amps

$\emptyset^I{}_{qr}$ is the *q*-axis rotor flux linkage referred to the main stator winding in Webbers

k is the turn ratio of N_a to N_m

ω_r is the rotor electrical angular velocity in rad/sec

i^I_{dr} is the *d*-axis rotor current referred to the main stator winding

$\emptyset^I_{dr}$ is the *d*-axis rotor flux linkage referred to the main stator winding

N_a is the number of auxiliary stator windings.

N_m is the number of main stator windings.

3.3.2 Model of the motor with constant parameters (Flux)

The equations that define the flux for the model (in the stationary reference frame *d*-*q*) are

$$\emptyset_{as} = L_{is} l q_s + L_{ms}\left(i_{qs} + i^I_{qr}\right) \quad (3.6)$$

$$\emptyset_{ds} = L_{ia} l_{ds} + k^2 L_{ms}(i_{ds} + i^I_{dr}) \quad (3.7)$$

$$\emptyset^I{}_{qr} = L^I_r l^I_{qr} + L_{ms}\left(i_{qs} + i^I_{qr}\right) \quad (3.8)$$

$$\emptyset^I{}_{dr} = k^2 L^I_{ir} l^I_{dr} + k^2 L_{ms}(i_{ds} + i^I_{dr}) \quad (3.9)$$

Where

L_{is} is the leakage inductance of the main stator winding

L_{ia} is the leakage inductance of the auxiliary stator winding.

L_{ms} is the magnetizing inductance of the main stator winding.

L^I_{ir} is the leakage inductance of the rotor winding referred to the main stator winding.

The electromagnetic torque expressed as a function of the rotor flux linkages and currents is

$$T_e = P\left(k.\emptyset_r^I l_{dr}^i - \frac{1}{k}.\emptyset_{qr}^I l_{qr}^I\right) \quad (3.10)$$

Where

T_e is the electromagnetic torque.

P is the number of pole pairs

3.3.3 Model of the motor with field-Oriented Control

Using the stator currents and rotor flux linkages as state-space variables for the SPIM model, the electromagnetic torque equation is

$$T_e = P.\frac{L_{ms}}{L_r^I}\left(\frac{1}{k}.l_{qs}\emptyset_{qr}^I - k.l_{ds}\emptyset_{qr}^I\right) \quad (3.11)$$

Using the next change of variable,

$$l_{qs} = k^2.i_{qs}I \quad (3.12)$$

And

$$l_{ds} = i_{ds}I \quad (3.13)$$

Therefore, the electromagnetic torque equation can be rewritten as

$$T_e = P.\frac{L_{ms}}{L_r^I}k\left(\emptyset_{dr}^I i_{qs1} - \emptyset_{qr}^I i_{ds1}\right) \quad (3.14)$$

In the indirect rotor flux-oriented control, the *d*-axis of the reference frame is oriented along the rotor flux linkage vector $\emptyset_r^I$, then

$$\emptyset_{dr}^I = \emptyset_r^I \quad (3.15)$$

And

$$\emptyset_{qr}^I = 0 \quad (3.16)$$

The electromagnetic torque results in

$$T_e = P.\frac{L_{ms}}{L_r^I}k.\emptyset_r ie_{qs1} \quad (3.17)$$

From here, the *q*-axis current component is

$$ie_{qs1} = \frac{T_e.L_r^I}{k.L_{ms}.P.\emptyset_r^I} \quad (3.18)$$

The resulting slip speed ω_s, is

$$\omega_s = \frac{k^3 L_{ms}.ie_{qs1}}{\left(\frac{L_r^I}{R_r^I}\right).\emptyset_r^I} \quad (3.19)$$

From here, the *d*-axis current component is

$$ie_{ds1} = \frac{\emptyset_r^I}{k^2 L_{ms}} \quad (3.20)$$

Where the *e is* superscript indicates that the variable is referred to the synchronous reference frame.

3.4 Models of the Single-phase Induction Motor

Figure 3.3 is used to write the models equation of the single-phase induction motor in arbitrarily frame.

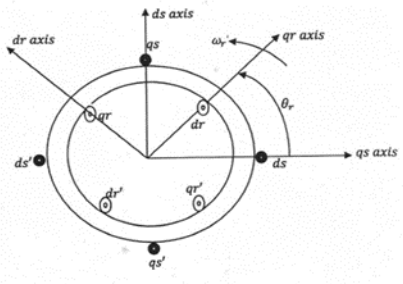

Figure 3.3: Rotor angular displacement in d-q frame

Assuming the turn ratio is 1, the stator and rotor voltage equation in d-q frame after transformation may be written as:

$$v_{qds} = r_s i_{qds} + \omega\lambda_{dqs} + P\lambda_{qds} \quad (3.21)$$

$$v_{qdr}' = r_r' i_{qdr} + (\omega - \omega r)\,\lambda_{dqr}' + P\lambda_{qdr}' \quad (3.22)$$

$$\lambda_{qs} = L_{ls} i_{qs} + L_{mq}(i_{qs} + i_{qr}') \quad (3.23)$$

$$\lambda_{ds} = L_{ls} i_{ds} + L_{md}(i_{ds} + i_{qr}') \quad (3.24)$$

$$\lambda_{qr}' = L_{lr} i_{qr}' + L_{mq}(i_{qs} + i_{qr}') \quad (3.25)$$

$$\lambda_{dr}' = L_{lr}' i_{dr}' + L_{md}(i_{ds} + i_{dr}') \quad (3.26)$$

Substituting equations (3.23) and (3.24) into (3.21) yields the stator d-q voltage equation in (3.27) and (3.28).

$$v_{qs} = r_r i_{qs} + \omega\lambda_{ds} + P(L_{ls} i_{qs} + L_{mq}\,(i_{qs} + i_{qr}')) \quad (3.27)$$

$$v_{ds} = r_r i_{ds} - \omega\lambda_{qs} + P(L_{ls} i_{ds} + L_{md} + (i_{ds} + i_{dr}')) \quad (3.28)$$

Similarly, substituting equations (3.25) and (3.26) into (3.22) yields the stator d-q voltage equation in (3.29) and (3.30)

$$v_{qr}' = r_r i_{qr}' + (\omega - \omega r)\lambda'_{dr} + P(L_{ls} i_{qs} + L_{mq}\,(i_{qs} + i_{qr}')) \quad (3.39)$$

$$v_{ds} = r_r i_{dr} - (\omega - \omega r)\lambda'_{dr} + P(L_{lr} i_{dr}' + L_{md}\,(i_{ds} + i_{dr}')) \quad (3.30)$$

Where:

V_{qs} is the *q*-axis stator voltage.

r_s is the main stator resistance.

i_{qs} is the *q*-axis stator current.

λ_{qs} is the *q*-axis stator flux linkage.

V_{ds} is the *d*-axis stator voltage.

i_{ds} is the *d*-axis stator current.

λ_{ds} is the *d*-axis stator flux linkage.

r'_r is the rotor winding resistance referred to the main stator winding.

i'_{qr} is the *q*-axis rotor current referred to the main stator winding.

λ'_{qr} is the *q*-axis rotor flux linkage referred to the main stator winding.

ω_r is the rotor electrical angular velocity.

ω is the stator electrical angular velocity.

i'_{dr} is the *d*-axis rotor current referred to the main stator winding.

λ'_{dr} is the *d*-axis rotor flux linkage referred to the main stator winding.

L_{ls} is the leakage inductance of the main stator winding.

L_{ms} is the magnetizing inductance of the main stator winding.

L'_{lr} is the leakage inductance of the rotor winding referred to the main stator winding.

The electromagnetic torque expressed as a function of the rotor flux linkages and currents is

$$T_e = 1.5P(\lambda_{qr} i_{dr} - \lambda_{dr} i_{qr}) \quad (3.31)$$

Where:

T_e is the electromagnetic torque.

P is the number of pole pairs.

The mechanical coupling equation relating to rotor speed in terms of developed electromagnetic torque is described as:

$$p\omega_r = \frac{P}{2J_T}(T_e - T_L) \tag{3.32}$$

Where

T_L is the load torque.

J_T is the combined moment of inertia of the rotor and the driving shaft.

This equivalent circuit that represents equations (3.21) through (3.31) is shown in Figure 3.5.

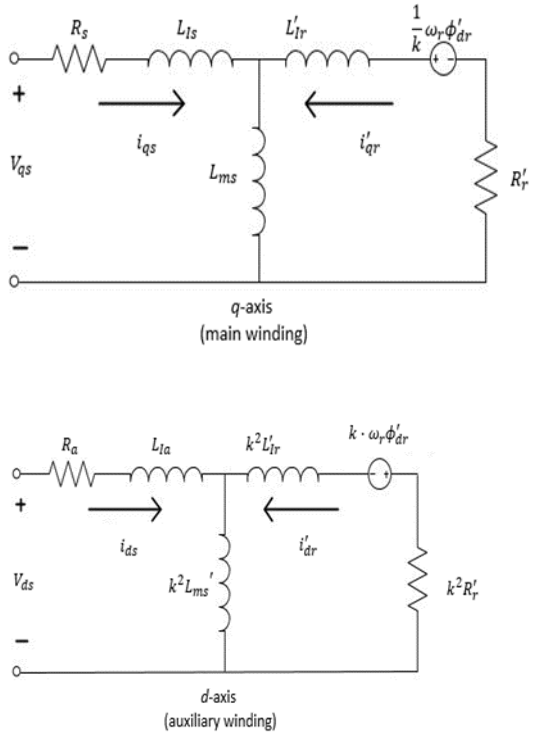

Figure 3.4: Auxiliary and main stator windings

3.5 Mode of Starting

To get the rotating magnetic field, the current in the auxiliary winding shall be displaced by 90° from the current in the main winding. This is achieved by connecting a capacitor in series with the auxiliary winding and parallel connection of the circuit to the main winding connected to the supply. For this reason, a suitable reactance is connected into the auxiliary winding (Figure 3.5).

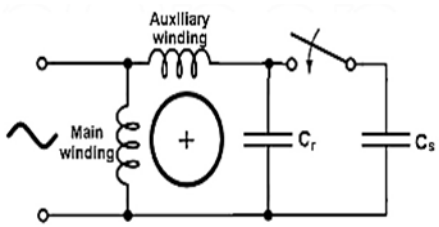

Figure 3.5: Starting modes of one-phase induction machine

The capacitor C_r connected into the auxiliary phase is optimally calculated according to the following equation:

$$C_r = 2200\ \frac{P_N}{U_N^2}\ [\mu F; W, V] \tag{3.33}$$

The one-phase induction motor is supplied by an alternating sinusoidal harmonic voltage that is generated by a simple harmonic oscillator in the model, having on its output the signal of harmonic voltage with the amplitude U_{1n} and frequency f_1 corresponding to the supply net. To achieve the starting torque, which is equal to the nominal, two to three times larger capacitor C_s is required, i.e.,

$$C_s = (2-3)C_r \tag{3.34}$$

3.6 The Single-phase Induction Motor Model

The motor model consists of models of electrical and mechanical parts. The electrical part is represented by the scheme in Figure 3.6.

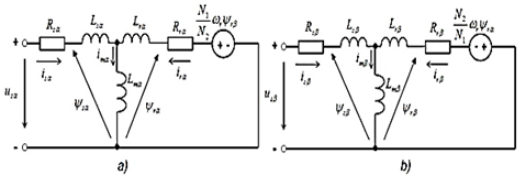

Figure 3.6: Equivalent circuits: (a) the main winding and (b) the auxiliary winding

Based on the equivalent circuits and dynamic equation of the motor, the model equations with their representations are illustrated below.

3.7.1 Model Equations for Stator Magnetic Flux

$$\psi_{s\alpha} = L_{s\alpha}\, i_{s\alpha} + L_{m\alpha} i_{r\alpha} \quad (3.35)$$

$$\psi_{s\beta} = L_{s\beta}\, i_{s\beta} + L_{m\beta}\, i_{r\beta} \quad (3.36)$$

3.7.2 Model Equations for Rotor Magnetic Flux

$$\psi_{r\alpha} = L_{m\alpha}\, i_{s\alpha} + L_{r\alpha} i_{r\alpha} \quad (3.37)$$

$$\psi_{r\beta} = L_{m\beta}\, i_{s\beta} + L_{r\beta}\, i_{r\beta} \quad (3.38)$$

3.7.3 Model Equations for Stator Current

$$i_{s\alpha} = \frac{1}{L_{s\alpha}} (\psi_{s\alpha} - L_{m\alpha} i_{r\alpha}) \quad (3.39)$$

$$i_{s\beta} = \frac{1}{L_{s\beta}} (\psi_{s\beta} - L_{m\beta} i_{r\beta}) \quad (3.40)$$

3.7.4 Model Equations for Rotor Current

$$i_{r\alpha} = \frac{1}{L_{r\alpha}} (\psi_{r\alpha} - L_{m\alpha} i_{r\alpha}) \quad (3.41)$$

$$i_{r\beta} = \frac{1}{L_{r\beta}} (\psi_{s\beta} - L_{m\beta} i_{s\beta}) \quad (3.42)$$

3.7.5 Model Equation for Motor Torque

$$M_m = P\left(\frac{N_1}{N_2}\psi_{r\beta} i_{r\alpha} - \frac{N_2}{N_1}\psi_{r\alpha} i_{r\beta}\right) \quad (3.43)$$

3.7.6 Model for Dynamic Equation

$$\frac{d\omega}{dt} = \frac{1}{J}.(M_m - M_{load}) \quad (3.44)$$

Table 3.1: Induction Machine parameters for Analysis

Parameters	Values
Phase Voltage (V_s)	220V
Stator Resistance (R_s)	74.02Ω
Rotor Resistance (R_r)	62.01Ω
Core Resistance (R_c)	0.6482Ω
Stator Leakage Inductance (L_{ls})	0.2084H
Rotor Leakage Inductance (L_{lr})	0.2084H
Magnetizing Inductance (L_{ms})	3.3477H
Number of poles	4
Frequency (f)	50Hz
Friction coefficient (B_m)	0.0000N-m .s/rad
Moment of Initial (J_m)	0.0025N-m .s^2/rad

Source: Research desk, Quality Control Laboratory, Alcon Construction Nig. Ldt.

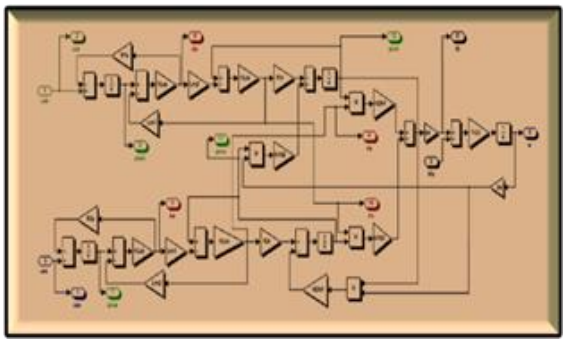

Figure 3.7: Simulink block diagram of one-phase induction motor

Figure 3.7 shows the Simulink block diagram which is use to determine the single-phase capacitor run induction motors of different components, the different characteristics (Supply voltage, motor torque, angular speed, stator current torque and stator current magnetic) of single-phase capacitor run induction motors, and the reverse direction of rotation of single-phase capacitor run induction motors.

VI. RESULTS AND DISCUSSION

The analyses discuss the results obtained from the single-phase induction motor simulation using MATLAB/Simulink. The results obtained from the simulation of the induction motor with a single connected capacitor and that of double capacitors are presented.

After the verification of the mathematical model of the single-phase motor by simulation, the designing and developing of the motor virtual model-graphical user interface was done in the MATLAB program, so that the user is granted simple handling in adjusting motor parameters and waveforms. Graphical user interface (GUI) allows one to visualize four different graphs: the input supply voltage, torque, angular velocity of the rotor, components of stator and rotor currents, and components of magnetic fluxes motor when starting the motor, during steady-state operation, and after loading it in the chosen time.

4.1 Solution of the Single Phase Induction Motor Model with Permanently Connected Single Capacitor

Simulation parameters:

U_1 = 230 V, f_1 = 50 Hz, M_{Load} = 5 Nm, C_r = 32 µF, T_{sim} = 0.8 s, T_{Load} = 0.5 s.

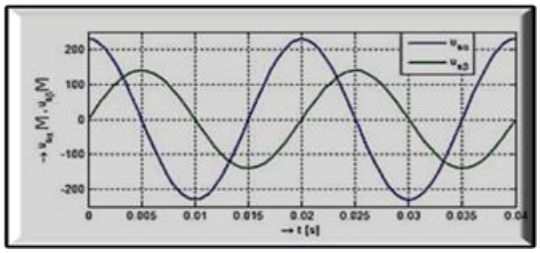

Figure 4.1: MATLAB Simulink Simulation result for supply voltages $u_{s\alpha}, u_{s\beta}$ of the motor with respect to time

Initially, the supply voltage for stator and rotor operates at 230V, For Stator scenario, when the time is = 0.1 seconds, the motor has no external load, because the voltage reduced to -220V at no-load value. When the time operates at t= 0.02 Second, the supply voltage increases to +220V. Similarly, When the time operates at t= 0.03 Second, the supply voltage decreases to -220V then finally, When the time operates at t= 0.04 Second, the supply voltage increases to +220V.

For rotor scenario, when the time is = 0.05 seconds, the motor has external load, because the voltage started point has a +120V with load value. When the time operates at t= 0.015 Second, the supply voltage reduced to -120V. Similarly, When the time operates at t= 0.025 Second, the supply voltage increases to +120V then finally, When the time operates at t= 0.0435Second, the supply voltage decreases to -120V.

The results show that the supply voltages operate at 230V and vary the load torque to find the maximum torque at this reduced voltage.

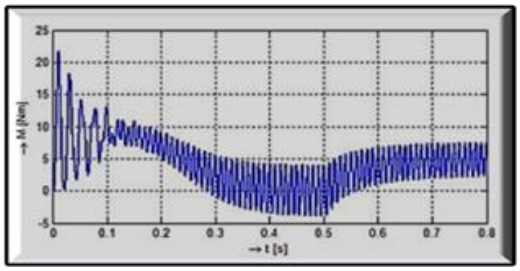

Figure 4.2: MATLAB Simulink Simulation result for motor torque M with respect to time

From our result the torque-speed envelope for the positive torque region only, that is, quadrants 1 and 4, when the maximum motor torque is 22 Nm and the minimum motor torque is 5 Nm vary with time from 0.02 seconds to 0.08 seconds, when the maximum motor torque is 12 Nm and the minimum motor torque is 8 Nm vary with time from 0.08 seconds to 0.1 seconds, when the maximum motor torque is 8 Nm and the minimum motor torque is 5 Nm vary with time from 0.1 seconds to 0.2 seconds, when the maximum motor torque is 5 Nm and the minimum motor torque is -2 Nm vary with time from 0.2 seconds to 0.3 seconds, when the maximum motor torque is 5 Nm and the minimum motor torque is 3.5 Nm vary with time from 0.3 seconds to 0.4 seconds, when the maximum motor torque is 4 Nm and the minimum motor torque is -4 Nm vary with time from 0.4 seconds to 0.5 seconds, when the maximum motor torque is 7 Nm and the minimum motor torque is 2Nm vary with time from 0.5 seconds to 0.6 seconds, when the maximum motor torque is 8 Nm and the minimum

motor torque is 3 Nm vary with time from 0.6 seconds to 0.7 seconds, when the maximum motor torque is 8.5 Nm and the minimum motor torque is 3.5 Nm vary with time from 0.7 seconds to 0.8 seconds.

If the speeds was positive (quadrant 1 or, equivalently, the motoring region), then the quadrant 4 torque envelope is defined by the block as the mirror image of quadrant 1. The motor torque-speed envelope has the same profile when the motor is operating in a reverse direction.

Finally, there will be electrical losses by using tabulated efficiency data, instead of a single efficiency measurement or tabulated loss data.

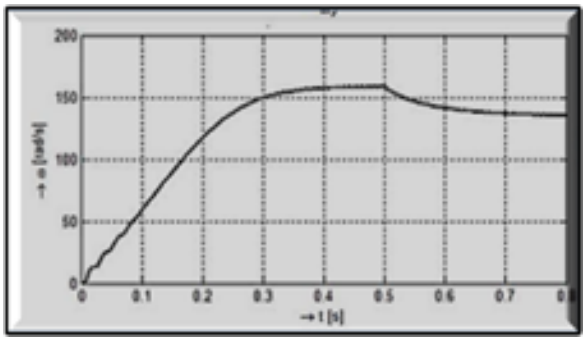

Figure 4.3: MATLAB Simulink Simulation result for angular speed ω with respect to time

From figure 4.3, it is seen that the plots have the different speed interval from of 155 rad/s. Also, they reach this steady state at the different time. The only obvious difference is noticed during the transient state, that is, between 0.1 to 0.8 second. The transient behavior is not exactly the same, but they are closely similar. This slight difference is as a result of the stator transients being neglected. It has, therefore, been shown that the stator transient can be used to predict the speed characteristics of an induction motor.

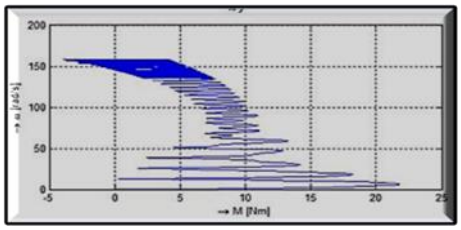

Figure 4.4: MATLAB Simulink Simulation result for static characteristic of the motor ω/M

The results relationship between static characteristic of the motor, the design shows that the system has a separated excitation DC motor fed by a chopper, there were some issues in stability of torque of DC motor, such as damping over shots, long rise time and fall time, and instability in system for interring and free load conditions.

When ω = 155 rad/s then M= oscillate from – 4 Nm and end at + 4 Nm, when ω = 148 rad/s then M= oscillate from 6 Nm and end at + 10 Nm, when ω = 100 rad/s then M= oscillate from 7 Nm and end at +10 Nm, when ω = 50 rad/s then M= oscillate from – 4 Nm and end at + 12 Nm.

Similarly, when ω = 45 rad/s then M= oscillate from 2.5 Nm and end at +10 Nm, when ω = 25 rad/s then M= oscillate from 2 Nm and end at +17 Nm and finally, when ω = 15 rad/s then M= oscillate from 0.5 Nm and end at +22 Nm.

However, the static characteristic of the motor operation of the system shows that there is an improvement on the system outputs very clear, such as reducing rising time after adding load from a given interval of time. We also notice that reducing the time to get stability after starting and after adding load will result to high efficiency of system and improvement the stability of the system.

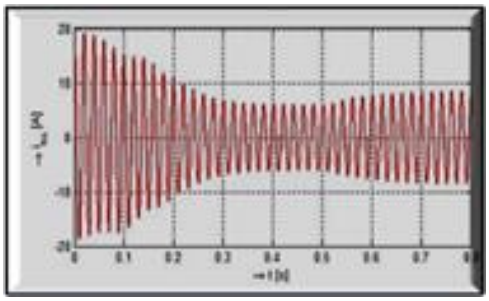

Figure 4.5: MATLAB Simulink Simulation result for stator currents: torque producing component $i_{s\alpha}$ with respect to time

From the result the MATLAB Simulink simulation result shows that the stator currents have stator transients. They have steady state value and they reach this value at the different time interval, starting from 0.10 second to 0.8 second. They have approximately different maximum and minimum values. The

transient characteristics are closely similar. Thus, we can conclude that the reduced model can be used effectively to determine the stator currents' characteristics of an induction motor.

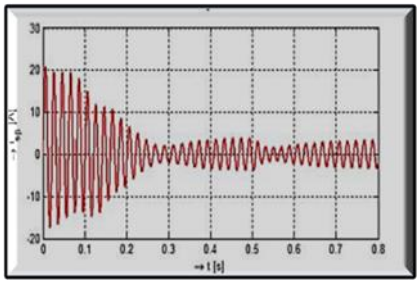

Figure 4.6: MATLAB Simulink Simulation result for stator currents: magnetic flow component $i_{s\beta}$ with respect to time

It can be seen from Figure 4.6 that the simulation results shows that the stator currents are very small. When the control target for the balanced stator current is applied the damped fundamental frequency components and DC components in the stator rotor currents have components in the d-axis fault component reference frame. Additionally, the amplitude of the DC component is not damped. In addition, the analytical expression for stator currents being based on the assumed condition that the voltage fluctuations during the grid fault conditions is neglected. In fact, when a fault occurs, there are oscillations in the terminal voltages due to the imbalance of the instantaneous power during the initial stage. This is the reason why the initial conditions of the calculated stator currents are different for the simulated stator currents.

4.2 Solution for a single-phase induction motor with a double capacitor

Simulation parameters**:**

U_1 = 230 V, f_1 = 50 Hz, M_{Load} = 5 Nm, C_s = 53 µF, C_r = 32 µF, $\omega_n = 110\frac{rad}{s}$, T_{sim} = 0.8 s, T_{Load} = 0.5 s.

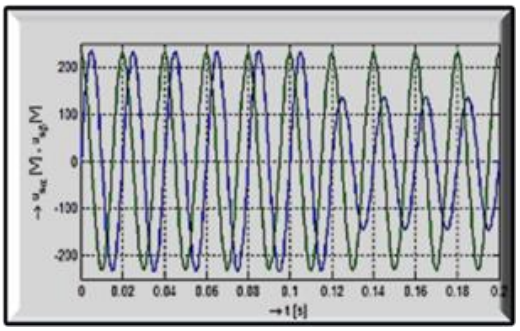

Figure 4.7: MATLAB Simulink Simulation result for double capacitor in respect to supply voltages $U_{s\alpha}$, $U_{s\beta}$ of the motor mode with respect to time

The above figure result for double capacitor in respect to supply voltages for the stator and rotor of the motor mode with respect to time. The result indicates that the stator voltage operate at maximum point of 100 rpm (rated speed) under no load. When the load is connected at 0.02 sec, the speed drops to about -220 rpm. When the wind speed increases to 120 rpm at 0.12 sec, there is a rapid increase in rotor speed. Then, the pitch controller starts operating to bring the rotor speed down to -120 rpm, which is the upper limit (+5%) of the frequency regulation band in the pitch controller.

For the rotor voltage operate at maximum point of 200 rpm (rated speed) under no load. When the load is connected at 0.02 sec, the speed drops to about -220 rpm, and maintained the frequency to 0.20 sec.

When the wind speed increases to 120 rpm at 0.12 sec, there is a rapid increase in rotor speed. Then, the pitch controller starts operating to bring the rotor speed down to -120 rpm, which is the upper limit (+5%) of the frequency regulation band in the pitch controller, this occurred as a result of damping over shots, long rise time and fall time, and instability in system for interring and free load conditions. However, after applying a double capacitor controller on the system of operation, you can notice the improvement on the system outputs very clear, such as reducing rising time after adding load from 0.02 second to 0.018 second.

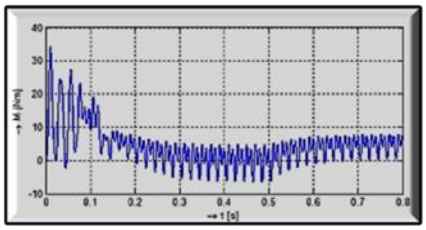

Figure 4.8: MATLAB Simulink Simulation result for double capacitor of the motor torque M with respect to time

As it is shown in figure 4.8, The MATLAB Simulink Simulation result for double capacitor of the motor torque with respect to time, the result shows that the starting load torque is controlled at a maximum value about 35Nm, and dropped at the minimum value of 18Nm at 0.1 second. After starting condition, the load torque is go down to about 10Nm due to absence of load on motor and decreases to -5Nm with the time interval between 0.2 seconds to 0.5 seconds. Then the load torque is loaded and the torque drawn from source increased to 8 Nm and continues to maintained the frequency without damping over shot and with very small rising interval of time between 0.5 seconds to 0.8 seconds, at steady state the double capacitor is applied as a result to stabilize the system effectively.

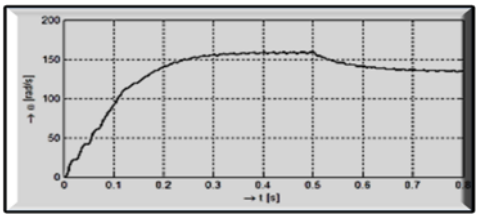

Figure 4.9: MATLAB Simulink simulation result for double capacitor with angular speed ω in respect to time

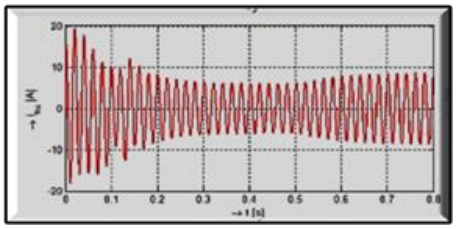

Figure 4.11: MATLAB Simulink Simulation result for double capacitor in respect to stator currents:

As can see in figure 4.9, the MATLAB Simulink simulation result for double capacitor with angular speed ω in respect to time under this supply condition, the no load dynamic performances are shown from 0 to 0.05 s, after which the angular speed is operate initially at the speed of 50 rad/s was applied. The dynamic response speed of the machine was increase at 100 rad/s as shown at 0.1 seconds, which was observed from the Figure traces that there is a smooth starting process. A high starting speed was increase from 145 rad/s at 0.2 seconds, and then it continue to increase to a speed of 150 rad/s at 0.3 seconds during the no load transient and then falls to 145 rad/s. The frequency of the speed was maintained and operates at the same speed rate of 150 rad/s at 0.5seconds. Then it gradually reduced to a speed level of 145 rad/s between the intervals of 0.6 seconds to 0.8 seconds.

To improve the motor performance during start period a higher capacity is required in the auxiliary phase circuit, therefore the double capacity is applied for the system to operate effectively.

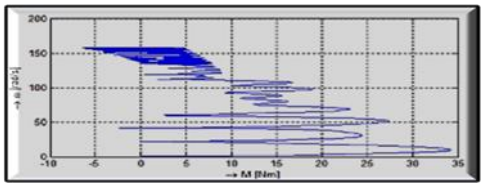

Figure 4.10: MATLAB Simulink Simulation of double capacitor of static characteristic of the motor $\omega = f(M)$ in respect to time

MATLAB Simulink Simulation of double capacitor of static characteristic of the motor with respect to time

Figure 4.10 shows MATLAB Simulink Simulation of double capacitor of static characteristic of the motor with respect to time. On application of the capacitor, the motor starts smoothly and the speed increased before the attainment of full nominal speed of 120 rad/sec at no load. This is the expected speed of a 4-pole 60Hz induction motor. At 5.0 seconds when the load torques was applied and as the load kept appreciating, the speed was maintained for a considerable time of 34.0 seconds before it starts subsiding to a full load speed of 155 rad/sec at allowable slip of 0.05.

torque producing component $i_{s\alpha}$ with respect to time

The machine result in Figure 4.11 shows the MATLAB Simulink Simulation of double capacitor of static characteristic of the motor with respect to time. The the main winding stator current plotted against time. When current is supplied to the machine, it starts with the main winding current of 19.0 A and drops to 10.0A at no-load, at time 0.10 second when load torque was applied and as the load appreciates; the machine maintained that value of current for a long time between the interval of 0.1seconds to 0.8 seconds before obtaining the full-load current. This shows the configuration of the windings is active due to the application of the capacitor.

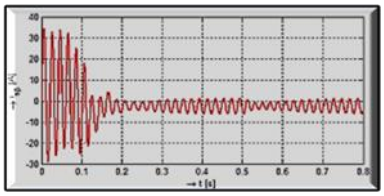

Figure 4.12: MATLAB Simulink Simulation result for double capacitor in respect to stator currents: magnetic flow component $i_{s\beta}$ with respect to time.

Figure 4.12 shows the MATLAB Simulink Simulation result for double capacitor in respect to stator currents: magnetic flow component with respect to time. The result obtained for plotting electromagnetic torque against time shows that the motor starts with a high starting torque, at 7.5Nm when the time is 0.1 second when load was applied and as it kept increasing, the electromagnetic torque kept appreciating in order to accommodate the load torque until it acquires a full-load torque of 35Nm at the interval of 0.1 second to 0.8 seconds.

The speed can be changed by the frequency, by changing the number of poles, and-in a small scale-by change of the voltage or value of the capacitor. The change of the direction of rotation is simply done by the pole change of the auxiliary winding. Time courses of the motor basic variables, motor torque, speed, and currents in both windings. The responses of the one-phase induction motor with the permanently connected capacitor and double-starting capacitor in the stator reference frame {α,β} at starting and loading the motor in the time 0.5s is used for the operation as illustrated in figures 4.1- 4.12.

In order to improve the motor performance during start period, a higher capacity is required in the auxiliary phase circuit. This is done by a capacitor C_s connected in parallel to the existing one up to the time instant the motor runs by speed about 70% ωN, which is followed by a centrifugal switch. After disconnecting, only the capacitor C_r of a lower value remains connected permanently.

All simulation results are taken with the constant load at acceleration. An extra load is added at 0.5 second in steady state. The transient and steady-state performances of the SPIM with an adjustable capacitor and double capacitors are shown in figures 4.7- 4.12. Acceleration of SPIM with double capacitor during starting period is higher than that of the SPIM with switching capacitor since SPIM with double capacitor uses a big starting capacitor value (32μF). However, the SPIM with double capacitor has better speed regulation in steady state operation. When the machine reaches to steady state operation, the load is increased at 0.5 s where the speed of the SPIM with double capacitor falls down much more than that of the SPIM with switching capacitor. This demonstrates better operating performance of the SPIM with double capacitor. The double capacitor produces higher torque in transient and steady state, and the efficiency of the motor with double capacitor is better in steady state operating region and reaches up to 85%.

CONCLUSION

This research work analyzes the optimization of single-phase induction motors for improved optimal control using a double capacitor control method is proposed. The suggested control method can be implemented with various control techniques. The motor at steady state was based on mechanical property.

The different characteristics (Supply voltage, motor torque, angular speed, stator current torque and stator current magnetic) of single-phase capacitor run induction motor were determined when a single and double capacitors were connected

A d-q equivalent circuit of the machine understudy was formulated and simulated using a matrix-laboratory (MATLAB) this was achieved using the machine d-q reference frame technique. The machine

input data were used and implemented into formulated machine variable for the study under investigation. The technique used characterized the voltage, current equation and torque expression which were used for the MATLAB/Simulink simulations. Basically the reactive power, (double capacitor) injected in the system shows improvement in the performance characteristics of the single-phase induction machine.

RECOMMENDATION

i. Apply a phase voltage of 230 V (motor rated voltage) to the terminals of the asynchronous motor and let the motor run.
ii. The machine should have a few more conductors in the stator and the increased power per current will result in a significant reduction in running costs in terms of low voltage, which will result in a reduction in watts per ampere.
ii. Motor power is transmitted through the main winding, which is stored in two-thirds of the stator slots and is supplied directly from the single-phase network. Therefore, the auxiliary winding must be designed for a lower current than the main winding.

REFERENCES

[1] Chomat, M. and Lipo, T. A. Adjustable-Speed Single-Phase IM Drive with Reduced Number of Switches. IEEE Transactions on Industry Applications, 39(3): 819-825, 2003.

[2] Jang, D. H. Problems Incurred in a Vector Controlled Single-Phase Induction Motor and a Proposal for a Vector-Controlled Two-Phase Induction Motor as a Replacement. IEEE Transactions on Power Electronics, 28(1): 526-536, 2013.

[3] Pawar, S. H. and Kulkarni, A. S. Design and Analysis of Sinusoidal PWM Inverter fed Fuel Pump Motor for High Horse-Power Locomotive in MATLAB. Global Journal of Engineering Science and Researches, 2(2): 23-29, 2015.

[4] Hekmati, P.; R. Yazdanpanah, J. M. Monfared and M. Mirsalim. Adjustable Capacitor for the SinglePhase IM Performance Improvement. IEEE Power Electronics, Drive Systems and Technologies Conference (PEDSTC 2014), Tehran, Iran: 7-12, 2014.

[5] Vabuderan, K., Rao, G.S. & Rao, P.S. (2015). Lecture note on Electrical Machines II' (pdf). 2-7.

[6] Obe, E.S. & Anih, L.U. Enhancement of the performance of a transfer field electric machine operating in the asynchronous mode, University of Nigeria, Nsukka, 2014.

[7] Ogunjuyigbe, A.S.O., Ayodede, T. R. & Adetokun, B.B. Modeling and analysis of a. dual stator winding induction machine Power, energy? machine and drive research group, electrical and Electronic Engineering Department, Faculty of Technology, University of Ibadan, Nigeria, 2018.

[8] Silong, K., Li, I. & Bulent, S. Double-ended synchronous reluctance motor derives with extended constant power speed ratio and increased power factor, Wisconsin electric machine and power electronics consortium (WEMPEC), University of Wisconsin-Madison, Wisconsin, USA, 2015.

[9] Akpama, E., J., Linus, A. & Ogbonnaya, O. Transient, analysis and modeling of six-phase asynchronous machine. American Journal of Electrical Power and Energy System, 77-83, 2015.

[10] Kouki, M. Fredj, M.B. & Rehaoulia, H. Research Laboratory SIME, ENS1T, University of Tunis, Tunisia, 56-1008, 2017.

[11] Mohscn, E. Mohammed, B., Bannes S. & Eborrhim, B. Modeling and synchronized control of dual parallel brush/ess direct current motors with single inverter. University of Tabirizm Iran, 2017.

[12] Obuah, E. & Inyenemi, M. Effect of design parameters on the performance of three phase induction motor. International Journal of Electrical Machines and Drives, 4(1), 2018.

[13] Ayodele, JT.R., Ogunjuyigbe, A.S.O. & Adetokun, B.B. Optimal capacitance selection for a wind-driven self-excited reluctance generator under varying wind-speed and load conditions. Power energy machine and drive (REMD), Electric Engineering Department, University of Ibadan, Nigeria, 2017.

[14] Bambang, P. Double fuzzy-Pi controller based speed control of permanent magnet synchronous motor University of. Bhayankara, Department of Electrical engineering, 2017.